ELSEVIER

Journal of Alloys and Compounds 303–304 (2000) 307–315

Journal of ALLOYS AND COMPOUNDS

www.elsevier.com/locate/jallcom

Near-infrared to visible photon upconversion processes in lanthanide doped chloride, bromide and iodide lattices

Hans U. Güdel*, Markus Pollnau

Department of Chemistry and Biochemistry, University of Bern, Freiestrasse 3, CH-3000 Bern 9, Switzerland

Abstract

The near-infrared to visible upconversion behavior of some selected Er^{3+}, Tm^{3+}, Dy^{3+} and Ho^{3+} doped chloride, bromide and iodide host lattices is summarized and discussed. The step from the well studied oxide and fluoride materials to the heavier halides can lead to dramatic changes in the upconversion behavior. This is mainly due to the lower vibrational energies which reduce the efficiency of multiphonon relaxation processes. As a consequence, new upconversion, cross-relaxation and luminescence processes become competitive. The relevance of these new materials lies in their potential for upconversion laser and phosphor applications.

Keywords: Upconversion; Lanthanides; Chloride; Bromide; Iodide; Optical spectroscopy

1. Introduction

Among the processes to convert near-infrared (NIR) to visible (VIS) or ultraviolet (UV) radiation, frequency conversion in nonlinear optical materials is the best known and most important. It requires coherent radiation of high intensity. Upconversion (UC) is a nonlinear process with a completely different physical basis, which mainly occurs in rare earth compounds. It is based on the presence of more than one electronically excited metastable state. The most simple situation is depicted schematically in Fig. 1: a ground state GS and two metastable excited states ES1 and ES2 with roughly equal energy spacings. The presence of the intermediate state ES1 in the NIR is essential. The three most important UC mechanisms are shown schematically in Fig. 1. A ground-state absorption (GSA) to ES1 is the first step in both mechanisms (a) and (b). It is followed by an excited state absorption (ESA) step ES1→ES2 in the GSA/ESA mechanism (a). In the GSA/ETU mechanism two centers excited to ES1 combine in a nonradiative energy transfer step to create an ES2 center (b). The particular feature of the avalanche process (c) is the absence of a GSA at the excitation wavelength and the presence of an efficient cross-relaxation populating the long-lived intermediate state ES1.

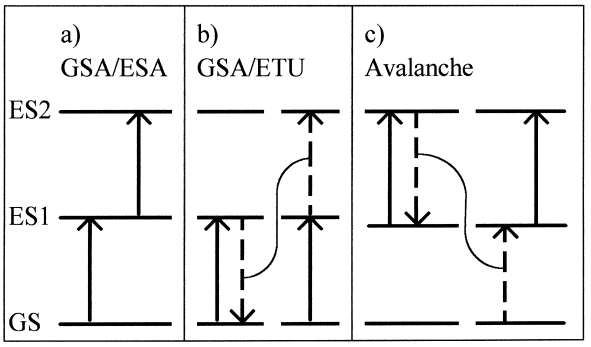

Fig. 1. Simple energy level diagram with ground state (GS) and two excited states (ES) indicating important upconversion mechanisms: (a) GSA/ESA; (b) GSA/ETU; (c) avalanche process.

The upconversion phenomenon is widespread among lanthanide compounds. There have also been reports of UC luminescence in uranium compounds. Among the transition metal ions UC has been reported in a few rare cases. The fundamentally different behavior of transition metal and rare earth metal ion systems can be explained by the more efficient shielding of the 4f and 5f electrons as compared to 3d, 4d or 5d electrons. The electron–phonon coupling is thus significantly smaller in rare earth compounds. As a consequence, multiphonon relaxation processes are less dominant, several f–f excited states can have finite lifetimes, and processes such as upconversion or cross-relaxation become competitive.

UC processes in lanthanide doped fluoride and oxide host materials, both crystals and glasses, have been most widely studied. The principal UC mechanisms in these

*Corresponding author.

0925-8388/00/$ – see front matter
PII: S0925-8388(00)00593-4

systems were already known and essentially understood 30 years ago [1,2]. In more recent years the research in this area was mainly driven by the potential application of upconversion materials in new light sources, such as lasers and phosphors. A number of upconversion lasers, both in fibers [3,4] and bulk crystals [5–7], have been reported in recent years.

We decided to explore lanthanide doped heavier halide materials for their UC behavior. Their lower vibrational energies are expected to further decrease the importance of multiphonon relaxation processes. As a consequence, upconversion as well as cross-relaxation (CR) processes become more competitive, and the excited state dynamics can be significantly different from that observed in the well-known oxides and fluorides. The examples presented in the following sections are from our own work. They are chosen to illustrate the most important UC properties of lanthanide doped chlorides, bromides and iodides. By studying the optical spectroscopic properties along the halide series we introduce a chemical coordinate into this research. If we can establish and understand a physical trend along the series, we may then be in a position to tune this physical property by chemical variation.

2. Physical trends along the halide series for Er^{3+} systems

Upconversion processes are ubiquitous among Er^{3+} compounds. Excitation around 810 or 980 nm leads to green luminescence around 550 nm in oxides and fluorides. Due to a favorable f–f energy level structure of Er^{3+} these processes can be highly efficient, and several UC lasers based on Er^{3+} activated fluoride materials have been reported [8–11]. In the heavier halides the UC behavior changes, and in the following the principal trends will be illustrated by examples and briefly discussed. The relevant UC excitation schemes are shown in Fig. 2.

2.1. Multiphonon relaxation

Fig. 3 compares the upconversion luminescence of 1% Er^{3+} doped $YAlO_3$ and $Cs_3Lu_2Br_9$ [12] after $^4I_{11/2}$ excitation around 980 nm at room temperature. Completely different behavior is evident. The yellow-green luminescence around 18 000 cm^{-1} corresponding to the $^4S_{3/2}\rightarrow{}^4I_{15/2}$ transition, is typical of oxides, fluorides and a number of chlorides. Iodides, bromides and a number of chlorides, on the other hand, show a green-blue luminescence just above 20 000 cm^{-1} which corresponds to a $^4F_{7/2}\rightarrow{}^4I_{15/2}$ transition. This is a typical result of increasing the mass of the ligands, leading to reduction of vibrational energies and thus a reduction of multiphonon relaxation rates.

In Fig. 4 we show Raman spectra of $Cs_3Er_2X_9$ (X=Cl, Br, I) [12]. The reduction of the highest vibrational energy

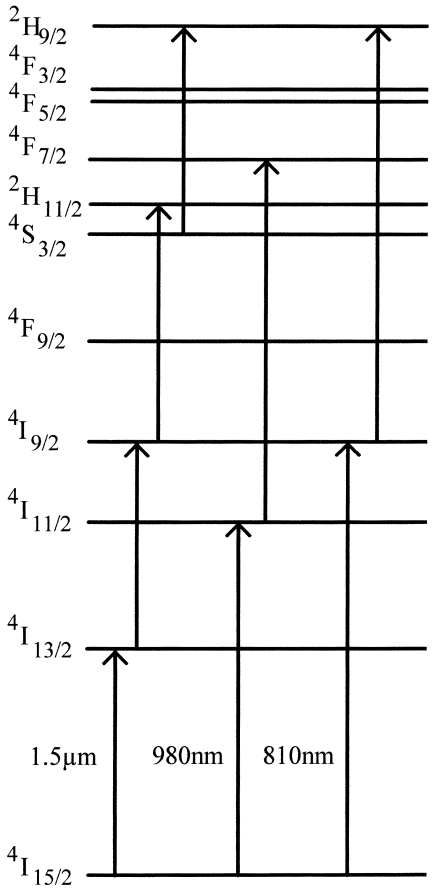

Fig. 2. Schematic energy level diagram of Er^{3+} up to 25 000 cm^{-1}, indicating possible upconversion steps under pump excitation at 1.5 μm (left), 980 nm (center), and 810 nm (right).

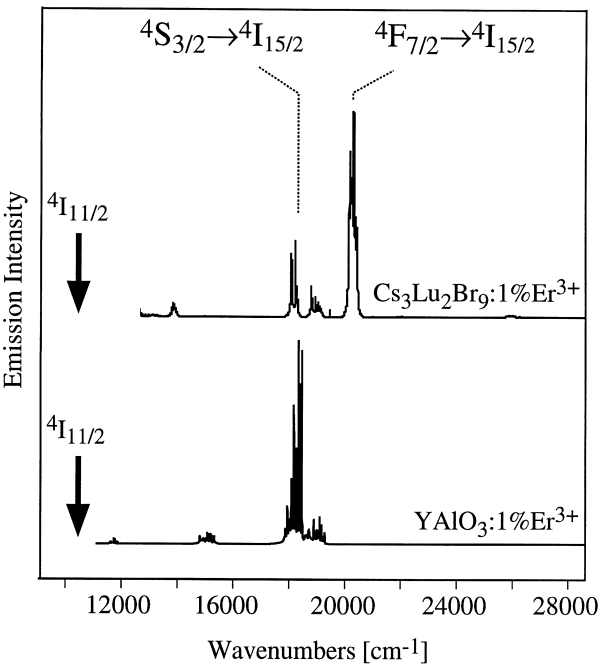

Fig. 3. Upconversion luminescence of $Cs_3Lu_2Br_9$ and $YAlO_3$ doped with 1% Er^{3+} at 295 K after $^4I_{11/2}$ excitation around 980 nm.

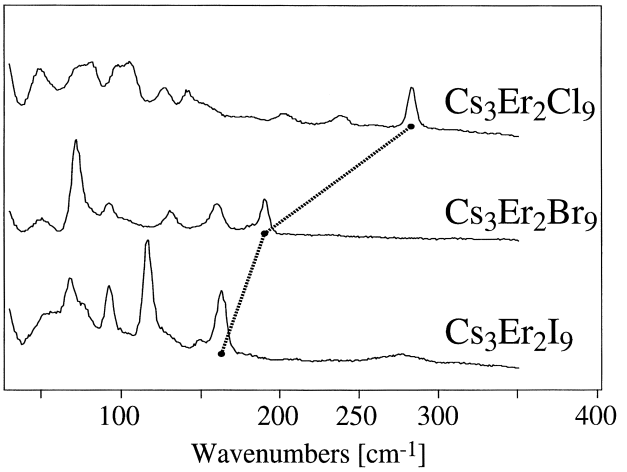

Fig. 4. Unpolarized Raman spectra, excited at 590.6 nm, for $Cs_3Er_2X_9$ (X=Cl, Br, I) at 295 K. The broken line indicates the variation of the highest-energy vibration frequency. (Figure reproduced from Ref. [12].)

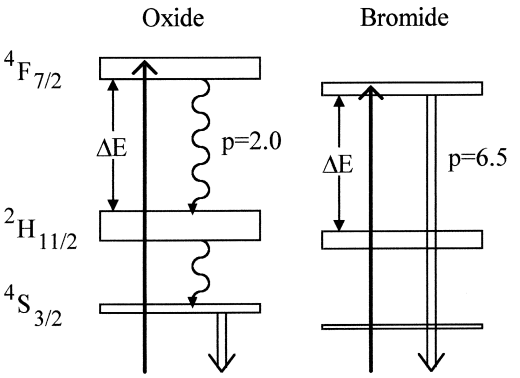

Fig. 5. Partial energy level scheme of Er^{3+} demonstrating the relevance of the energy gap law for the occurrence of $^4S_{3/2}\rightarrow{}^4I_{15/2}$ and $^4F_{7/2}\rightarrow{}^4I_{15/2}$ emission. p is the number of highest-energy phonons required to bridge the $^4F_{7/2}$–$^2H_{11/2}$ energy gap.

from 285 to 190 and 160 cm^{-1} for X=Cl, Br and I, respectively, can be nicely followed. In Table 1 typical energies for the highest-energy vibration in oxide and halide lattices are listed. The dependence of the multiphonon relaxation rate constant across an energy gap ΔE between f–f states on the vibrational energy is well described by the energy gap law [17]:

$$k_{mp} = C \cdot e^{-p\beta} \quad (1)$$

where C and β are positive constants characteristic of the material. p is defined as

$$p = \frac{\Delta E}{\hbar\omega_{max}} \quad (2)$$

i.e. the number of highest-energy vibrational quanta required to bridge the energy gap. As a rule of thumb for 4f systems multiphonon relaxation processes according to Eq. (1) are competitive up to about $p = 5$–6. Fig. 5 shows the relevant part of the energy level scheme of Er^{3+}. After direct or upconversion ($^4I_{15/2}\rightarrow{}^4I_{11/2}\rightarrow{}^4F_{7/2}$ around 980 nm) excitation the relevant energy gap for relaxation is between $^4F_{7/2}$ and $^2H_{11/2}$. With the $\hbar\omega_{max}$ and ΔE values listed in the first and second column of Table 1, respectively, the p values in the third column are obtained using Eq. (2). With p values of 2.0 and 6.5 for oxide and bromide, respectively, we expect $^4F_{7/2}\rightarrow{}^2H_{11/2}$ multiphonon relaxation to be dominant in the oxide and less important in the bromide. This corresponds to the observed behavior (see Fig. 3).

Table 1
Typical energies of highest-energy vibrations in trivalent oxide and halide lattices ($\hbar\omega_{max}$). Values of the energy gaps ΔE between the $^4F_{7/2}$ and $^2H_{11/2}$ multiplets in Er^{3+} systems are derived from the energy level data of Refs. [13–16]. The number p of phonons required to bridge this energy gap is given in the third column

		$\hbar\omega_{max}$ (cm^{-1})	ΔE (cm^{-1})	p
Oxide	($YAlO_3$)	600	1178	2.0
Fluoride	($LiYF_4$)	400	1227	3.1
Chloride	($Cs_3Lu_2Cl_9$)	285	1215	4.3
Bromide	($Cs_3Lu_2Br_9$)	190	1227	6.5
Iodide	($Cs_3Y_2I_9$)	160	1234	7.7

$^4I_{11/2}$ is the most widely used intermediate state SE1 for NIR to VIS upconversion in Er^{3+} systems (see Fig. 2). Since the absorption cross-section for the $^4I_{15/2}\rightarrow{}^4I_{11/2}$ GSA transition is very small this step is often sensitized by Yb^{3+}. The change in the upconversion luminescence wavelength from about 550 to 490 nm between an oxide and a bromide is significant, both in terms of potential laser and phosphor applications. Excitation into $^4I_{9/2}$ around 810 nm leads to efficient $^2H_{9/2}\rightarrow{}^4I_{15/2}$ UC luminescence around 410 nm in bromides (see Fig. 2 and Ref. [18]). In fluorides and oxides both the intermediate state $^4I_{9/2}$ and the emitting state $^2H_{9/2}$ suffer from competitive nonradiative deactivation.

2.2. Upconversion after 1.54 μm excitation [19]

The most intense absorption band of Er^{3+} in the NIR is due to the $^4I_{13/2}$ excitation around 1.5 μm. We have studied the UC behavior of Er^{3+} doped $Cs_3Lu_2Cl_9$, $Cs_3Lu_2Br_9$ and $Cs_3Y_2I_9$ for this excitation in detail. An overview of the results is presented in Fig. 6. Luminescence up to the near-UV is observed in the chloride and bromide host lattices. As a result of the very favorable energy level structure of Er^{3+}, up to four 1.5 μm quanta can be added in the following consecutive upconversion steps:

$$^4I_{15/2}\rightarrow{}^4I_{13/2}\rightarrow{}^4I_{9/2}\rightarrow{}^2H_{11/2}/{}^4S_{3/2}\rightarrow{}^2H_{9/2}$$

(see Fig. 2). This behavior is distinctly different from that observed in fluoride and oxide host lattices, mainly because of the lack of $^4I_{9/2}\rightarrow{}^4I_{11/2}$ nonradiative relaxation in the heavier halides. The $^4I_{9/2}$–$^4I_{11/2}$ energy gap is

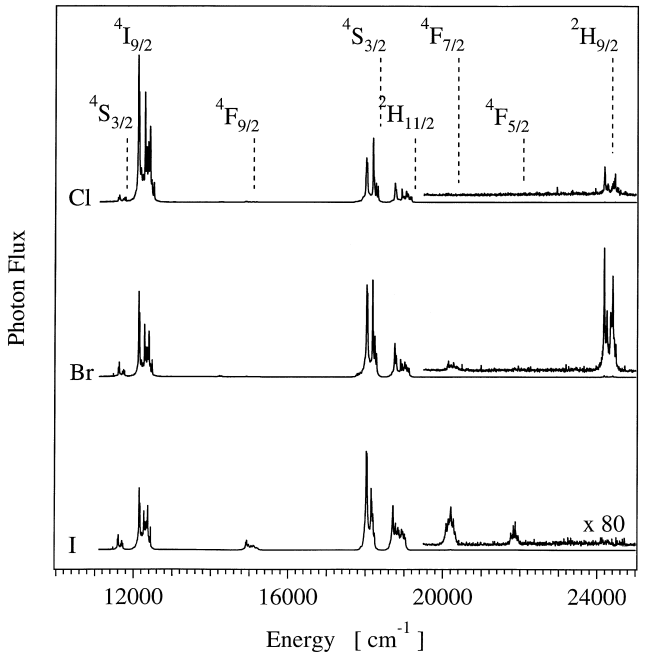

Fig. 6. Unpolarized upconversion luminescence spectra of $Cs_3Lu_2Cl_9$ (top), $Cs_3Lu_2Br_9$ (middle), and $Cs_3Y_2I_9$ (bottom) doped with 1% Er^{3+} at 295 K. The samples are excited at 1.54 μm by the $^4I_{15/2}\rightarrow{}^4I_{13/2}$ transition. The labeled transitions terminate on the $^4I_{15/2}$ ground-state multiplet except for the $^4S_{3/2}\rightarrow{}^4I_{13/2}$ transition around 11 700 cm^{-1}. (Figure reproduced from Ref. [19].)

typically 1894, 2036, 2117, 2135 and 2138 cm^{-1} in oxide, fluoride, chloride, bromide and iodide lattices, respectively. Since the energy of the highest optical phonons drops by 75% along this series, the multiphonon relaxation rate constant k_{mp} drops by orders of magnitude along this series according to the energy gap law of Eq. (1). Between fluoride and chloride the relative importance of radiative and multiphonon relaxation of $^4I_{9/2}$ reverses. As a consequence, processes such as cross-relaxation and upconversion from this level become competitive. It is interesting that, in the $Cs_3Y_2I_9$ host lattice, even the energy gap between $^2H_{11/2}$ and $^4S_{3/2}$ of 669 cm^{-1} is large enough to prevent thermalization of the two states. Despite the fact that p is only 4.2, radiative relaxation $^2H_{11/2}\rightarrow{}^4I_{15/2}$ is competitive because of its very large oscillator strength.

2.3. Power dependence of upconversion luminescence intensities

If an upper excited state is mainly populated by a dominant UC process from an intermediate state, the dependence of the UC luminescence intensity on the pump power is governed by the competition of a linear decay rate with the nonlinear UC rate for the depletion of the intermediate state. If the UC rates are negligible compared to the linear decay rates from the corresponding intermediate states for several successive UC steps, the order n of the excitation process, i.e. the number of photons n required for the excitation of the corresponding emitting level, is indicated by the slope of the luminescence intensity versus pump power in double-logarithmic representation. A completely different situation obtains if nonlinear UC rates dominate over linear decay rates for the depletion of the intermediate states. The slope in the power dependence of luminescence from the highest-lying state is then expected to converge to one, whereas the slopes of luminescences from intermediate excited states are expected to converge to values smaller than one [20].

Fig. 7a,b show measured power dependencies of various UC luminescence transitions to the $^4I_{15/2}$ ground-state multiplet after 1.54 μm excitation in $Cs_3Lu_2Cl_9$:1% Er^{3+} and $Cs_3Er_2Cl_9$ at 77 K, respectively [19]. The condition

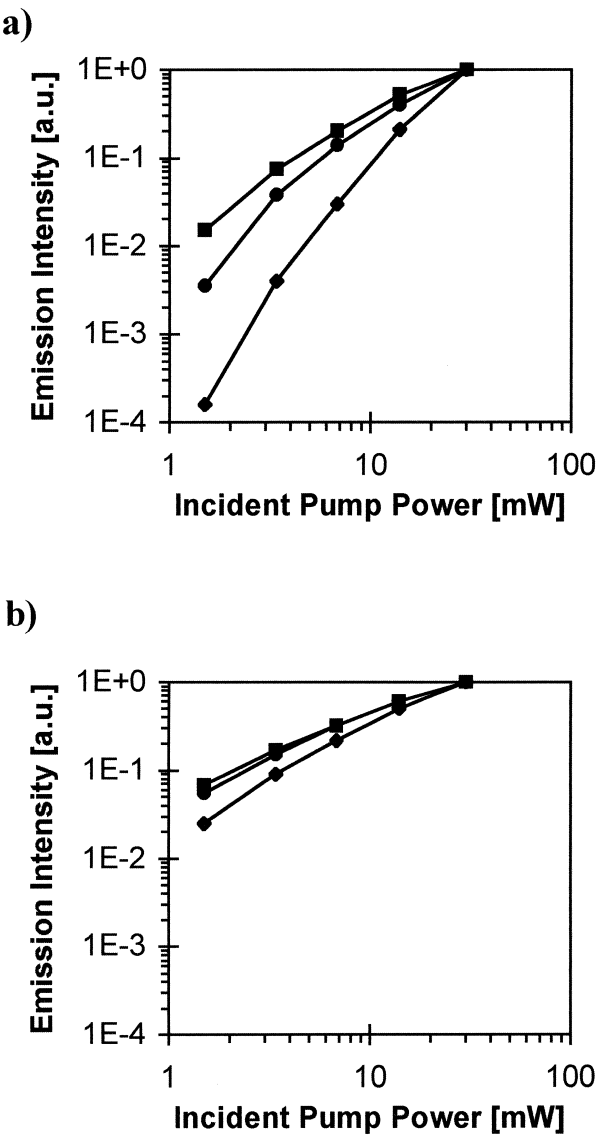

Fig. 7. Power dependence of upconversion luminescence from $^4I_{9/2}$ (squares), $^4S_{3/2}$ (circles), and $^2H_{9/2}$ (diamonds) in (a) $Cs_3Lu_2Cl_9$:1% Er^{3+} and (b) $Cs_3Er_2Cl_9$. The Er^{3+} ions were excited at 1.54 μm by the $^4I_{15/2}\rightarrow{}^4I_{13/2}$ transition. (Figure modified from Ref. [19].)

that UC rates are negligible compared to the linear decay rates of the intermediate states is approximately fulfilled for the 1% sample at low pump power, because the excitation density is small. The initial slopes measured in $Cs_3Lu_2Cl_9$:1% Er^{3+} (Fig. 7a) are close to 2, 3 and 4 for the $^4I_{9/2}$, $^4S_{3/2}$ and $^2H_{9/2}$ luminescences, respectively. This suggests a two-step UC process for the population of $^4I_{9/2}$, a three-step process for $^4S_{3/2}$, and a four-step process for $^2H_{9/2}$, as expected for the excitation sequence

$$^4I_{15/2} \rightarrow {}^4I_{13/2} \rightarrow {}^4I_{9/2} \rightarrow {}^4S_{3/2}/{}^2H_{11/2} \rightarrow {}^2H_{9/2}$$

(see Fig. 2).

However, in $Cs_3Lu_2Cl_9$:1% Er^{3+} at higher pump powers and clearly in $Cs_3Er_2Cl_9$ the slopes deviate significantly from these values. The measured slope (Fig. 7b) for the $^2H_{9/2}$ luminescence in $Cs_3Er_2Cl_9$ converges to one at higher pump power, whereas the slopes of the luminescence intensities from intermediate excited states converge to values smaller than one. In $Cs_3Er_2Cl_9$ the excitation density is high. Consequently, the main ETU processes have higher rates than the luminescent processes, which leads to the observed behavior.

3. Upconversion processes involving Yb^{3+}

The Yb^{3+} ion with a $4f^{13}$ electron configuration takes a very special position within the lanthanide series. It has only one f–f excited state around 1 μm, and between this NIR absorption and the onset of the first ligand-to-metal charge-transfer excitations in the UV it is transparent. This has two important consequences. Yb^{3+} systems are eminently suited to observe and study so-called cooperative upconversion processes, in which two 1 μm excitations on neighboring Yb^{3+} ions combine to create a green luminescence. This has been observed in a number of Yb^{3+} compounds. In Yb^{3+} doped $Cs_3Y_2Br_9$, $Cs_3Lu_2Br_9$ and $CsCdBr_3$ this luminescence exhibits the very interesting phenomenon of intrinsic optical bistability [21].

The example to be presented here concerns the second consequence of the very special energy level structure of Yb^{3+}. Several NIR to VIS lanthanide upconversion systems can be efficiently sensitized by Yb^{3+} ions. We have studied Tm^{3+} doped $Cs_3Yb_2Cl_9$ and used the host as a sensitizer [22]. Excitation of the $^2F_{7/2} \rightarrow {}^2F_{5/2}$ transition of Yb^{3+} around 940 nm leads to Tm^{3+} emissions throughout the VIS and near-UV, as shown in Fig. 8. The corresponding UC excitation scheme is shown in Fig. 9. Up to four Yb^{3+} excitations can be injected into one Tm^{3+} ion. The excitation is mobile within the $Cs_3Yb_2Cl_9$ lattice, it can thus readily reach the Tm^{3+} traps. Excitation of Tm^{3+} occurs by nonradiative energy transfer. This is very efficient due to the short distance of 3.6 Å between the two ions in the $TmYbCl_9^{3-}$ dimers present in this lattice. Similar observations have been made in Tm^{3+} doped fluoride crystals. The relevance of these systems lies in the

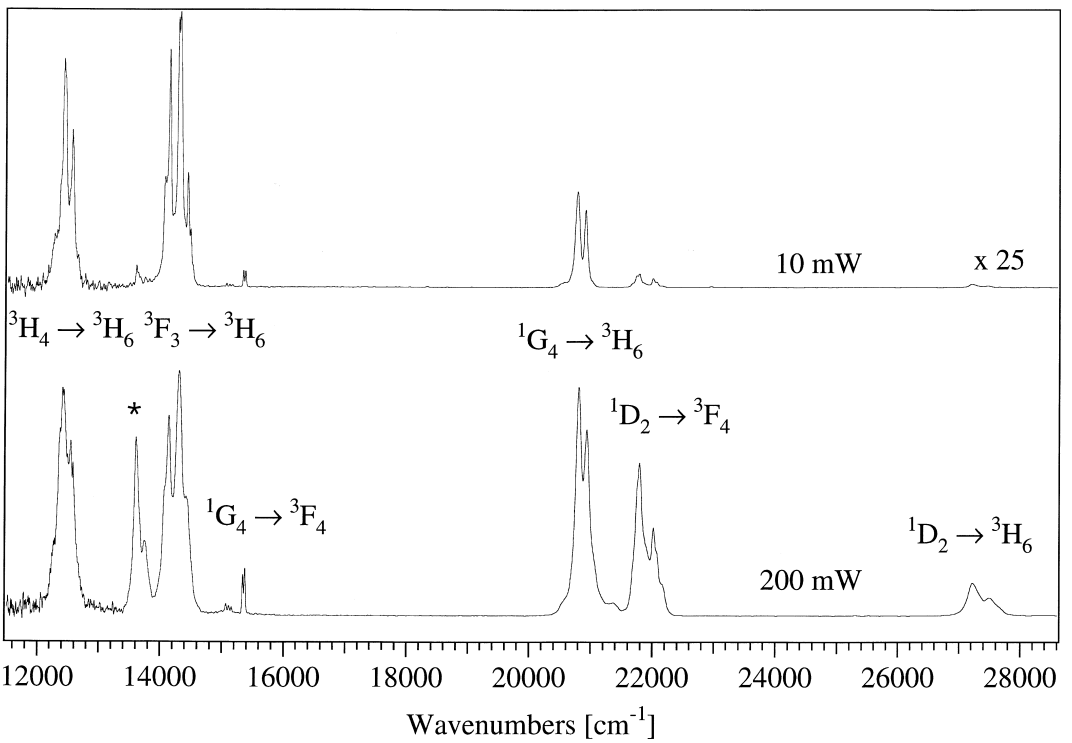

Fig. 8. Upconversion luminescence spectra of $Cs_3Yb_2Cl_9$:5% Tm^{3+} at 10 K with two different pump intensities at 10 670 cm^{-1}: 10 mW (upper trace) and 200 mW (lower trace). The upper trace is multiplied by a factor of 25. The peak labeled with an asterisk is the second order of the $^1D_2 \rightarrow {}^3H_6$ luminescence. (Figure reproduced from Ref. [22].)

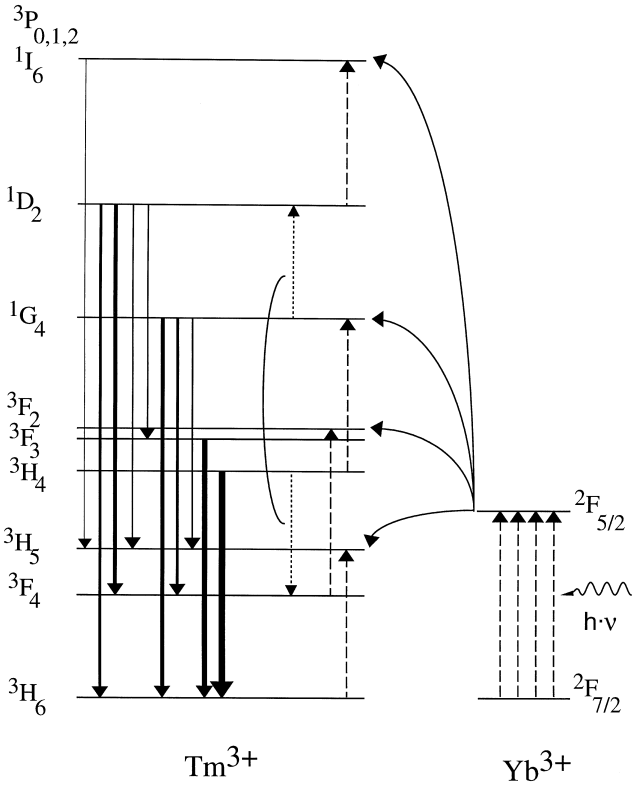

Fig. 9. Schematic diagram of possible upconversion processes and observed VIS/UV luminescence in $Cs_3Yb_2Cl_9$:5% Tm^{3+}. The broken arrows show the sequential $Yb^{3+} \rightarrow Tm^{3+}$ energy transfer steps. The dotted arrows indicate an upconversion process within the Tm^{3+} system. (Figure reproduced from Ref. [22].)

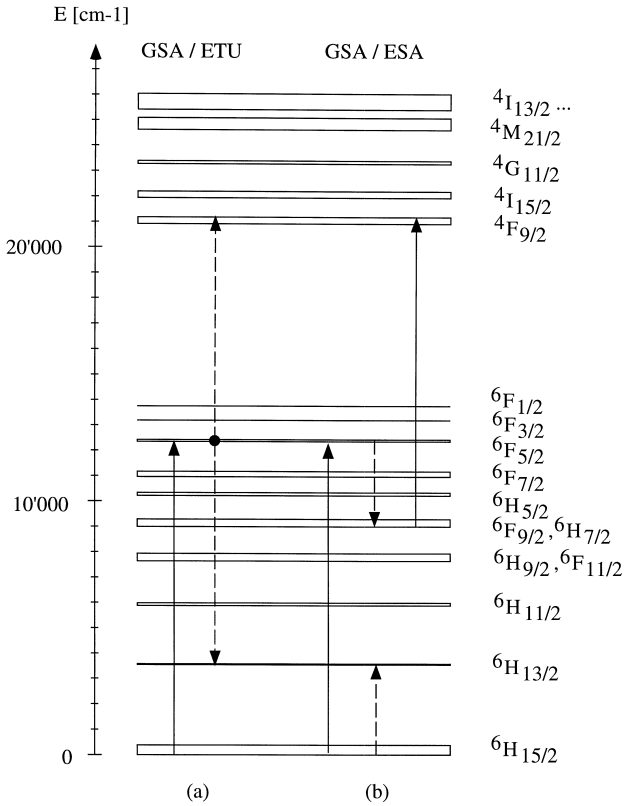

Fig. 10. Energy level diagram of Dy^{3+} showing possible GSA/ETU and GSA/ESA mechanisms to populate $^4F_{9/2}$ after $^6F_{5/2}$ excitation. The cross-relaxation step preceding ESA is indicated with dashed arrows. (Figure modified from Ref. [23].)

high total efficiency of the process and the high relative intensity of the two blue emissions $^1G_4 \rightarrow {}^3H_6$ around 21 000 cm^{-1} and $^1D_2 \rightarrow {}^3F_4$ around 22 000 cm^{-1}. There is a potential for using these in both laser and phosphor applications.

4. Mechanism of upconversion processes in Dy^{3+} and Ho^{3+} doped $CsCdBr_3$ [23,24]

Dy^{3+} does not belong to the lanthanide ions for which UC luminescence has been reported so far. And inspection of the energy level scheme in Fig. 10 reveals the reason. There are a number of relatively densely packed energy levels in the NIR, and excitation into any of the states between 8000 and 14 000 cm^{-1} will be immediately followed by multiphonon relaxation processes. Incorporating Dy^{3+} into the host lattice $CsCdBr_3$ with a maximum phonon energy of 163 cm^{-1} alters the situation [22]. The energy gap between $^6F_{5/2}$ and $^6F_{7/2}$ (see Fig. 10) is about 1300 cm^{-1} and thus large enough to significantly slow down the multiphonon relaxation. $^6F_{5/2}$ in Dy^{3+} doped $CsCdBr_3$ has a lifetime of 1.2 ms at 10 K. As a consequence, UC luminescence is observed throughout the VIS upon $^6F_{5/2}$ and $^6F_{3/2}$ excitation (see Fig. 11). The most intense luminescence bands are due to transitions originating in $^4F_{9/2}$. We can now proceed to determine the mechanism by which this upconversion is achieved. This is done by considering the UC excitation spectra monitoring the $^4F_{9/2} \rightarrow {}^6H_{13/2}$ luminescence shown in Fig. 12. At

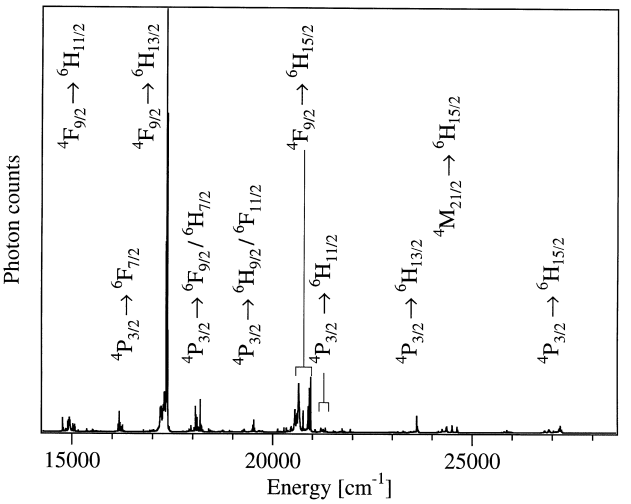

Fig. 11. Survey upconversion luminescence spectrum of $CsCdBr_3$:1% Dy^{3+} at 10 K using $^6F_{5/2}$ excitation at 12 338 cm^{-1}. (Figure reproduced from Ref. [23].)

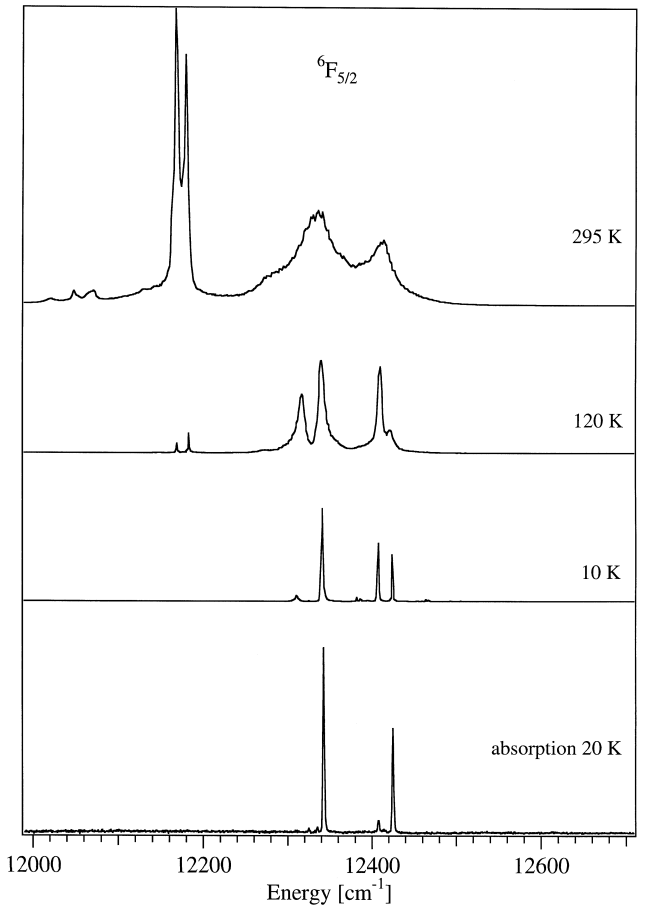

Fig. 12. Upconversion excitation spectra of $CsCdBr_3$:1% Dy^{3+} at three temperatures detecting the intense $^4F_{9/2}\rightarrow{}^6H_{13/2}$ luminescence at 17 341 cm^{-1}. The individual spectra are scaled to an equal height of the peak at 12 338 cm^{-1}. The absorption spectrum at 20 K of the same spectral region is shown at the bottom. (Figure modified from Ref. [23].)

temperatures below 100 K the excitation spectrum between 12 000 and 12 500 cm^{-1} corresponds to the $^4F_{5/2}$ ground-state absorption spectrum. Above 100 K and up to room temperature two new and intense lines at 12 164 and 12 177 cm^{-1} arise on the low-energy side of the excitation spectrum, which have no counterparts in the GSA spectrum. This is a clear indication of an ESA upconversion mechanism. Analysis of the hot line positions reveals that they correspond to a $^6F_{9/2}\rightarrow{}^4F_{9/2}$ ESA (see right-hand side of Fig. 10). This surprising result can be understood as shown in Fig. 10b. The $^6F_{5/2}$ excitation is followed by an efficient cross-relaxation step to $^6F_{9/2}$, from which $^6F_{9/2}\rightarrow{}^4F_{9/2}$ ESA can occur. A Judd–Ofelt calculation gives a high oscillator strength $f = 2.1\times10^{-6}$ for this transition. At 10 K there is no GSA at 12 164 and 12 177 cm^{-1}, and the sequence GSA/cross-relaxation/ESA cannot work. Above 100 K, however, there is some nonvanishing GSA at these energies, and the sequence can take place. This very interesting UC mechanism is supported by the observation that no UC could be induced at these two wavelengths using pulsed excitation with 10 ns pulse width. The nonradiative cross-relaxation step is slow compared to this pulse width, i.e. $k_{cr} < 10^8$ s^{-1}, and thus the ESA step cannot take place within the pulse duration.

In the above example the UC excitation spectrum was used to discriminate between GSA/ETU and GSA/ESA upconversion mechanisms. Another way to distinguish between these two major UC mechanisms is by observing the time evolution of a UC luminescence after a pulsed excitation. We use Ho^{3+} doped $CsCdBr_3$ to illustrate this [24]. There is a metastable $^5I_5$ multiplet in the NIR around 11 200 cm^{-1} which can be used to induce UC luminescence from the $^5F_3$ multiplet around 21 000 cm^{-1}. The excitation spectrum of this UC luminescence is depicted in Fig. 13. Similar to the situation in Dy^{3+} doped $CsCdBr_3$ discussed above, there are excitation lines corresponding to the GSA. Between 100 and 295 K, however, the excitation spectrum is dominated by hot bands at lower energy (see the shaded bands in Fig. 13). Their energies correspond to $^5I_5\rightarrow{}^5F_3$ ESA transitions, and we have a very strong case for a hot GSA/ESA upconversion sequence. This is now confirmed by the time dependence of the $^5F_3\rightarrow{}^5I_8$ luminescence intensity at 100 K after an excitation pulse at 11 028 cm^{-1} (shaded area of Fig. 13) and 11 232 cm^{-1} (unshaded area). It is shown in Fig. 14a,b, respectively. The intensity shows up instantaneously after the pulse and decays exponentially in Fig. 14a. This is a clear signature of a GSA/ESA sequence taking place within the 10 ns duration of the pulse. In contrast, the time dependence in Fig. 14b exhibits a rise within the first 300 μs which is then followed by a similar decay as in Fig. 14a. This is the typical behavior of a GSA/ETU process. The rise time of the UC luminescence is determined by either the lifetime of the intermediate state combined with the rate constant of the energy transfer step or the lifetime of the emitting state. In the present case it is the former, and from the experimental rise time of 168 μs a rate constant $W_t = 5815$ s^{-1} was derived for the energy transfer process.

5. Conclusions

Despite the fact that the electronic structure of the lathanides does not strongly depend on the chemical environment, the NIR to VIS photon upconversion behavior can be strongly influenced by varying the lanthanide coordination along the halide series. The main effect is a reduction of lanthanide–halide vibrational energies along F–Cl–Br–I. As a consequence, the importance of nonradiative multiphonon relaxation processes diminishes. Electronic states which are immediately depleted by multiphon relaxation in oxides or fluorides become metastable in chlorides and bromides. This opens new pathways for upconversion processes, alters excited state dynamics and can lead to a completely new upconversion behavior compared to the well-studied behavior in oxide and

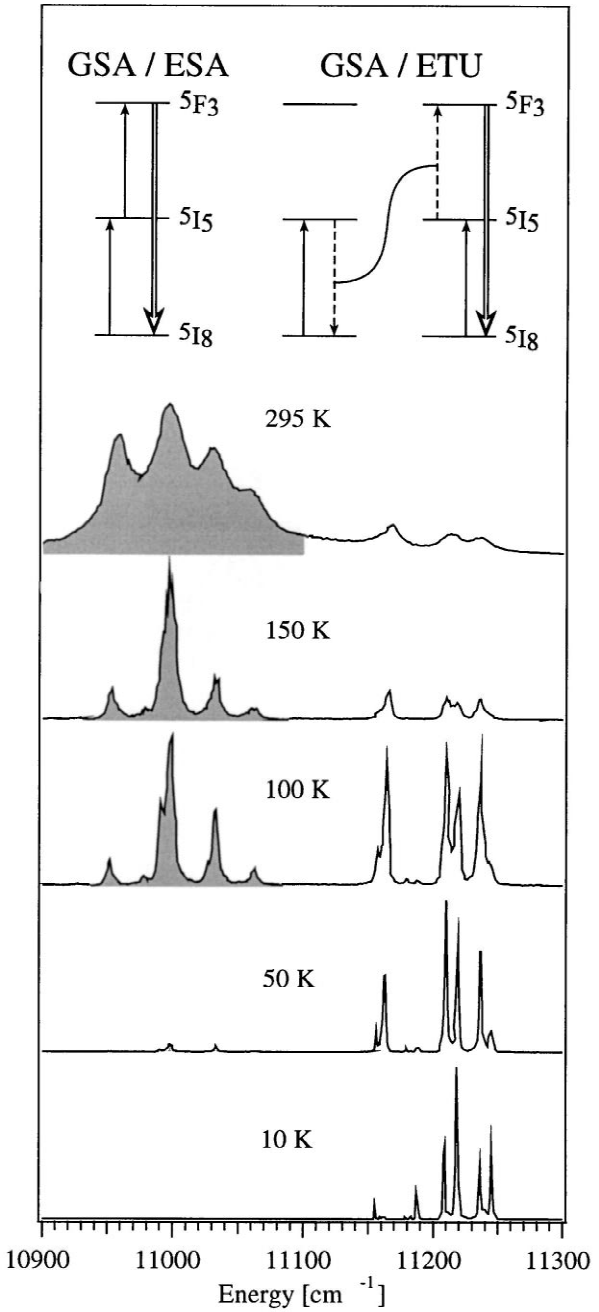

Fig. 13. Upconversion excitation spectra of $CsCdBr_3$:2.25% Ho^{3+} as a function of temperature. The shaded and unshaded excitation regions correspond to different upconversion mechanisms as shown schematically at the top. The 295 K spectrum is enlarged by a factor of 10. (Figure modified from Ref. [24].)

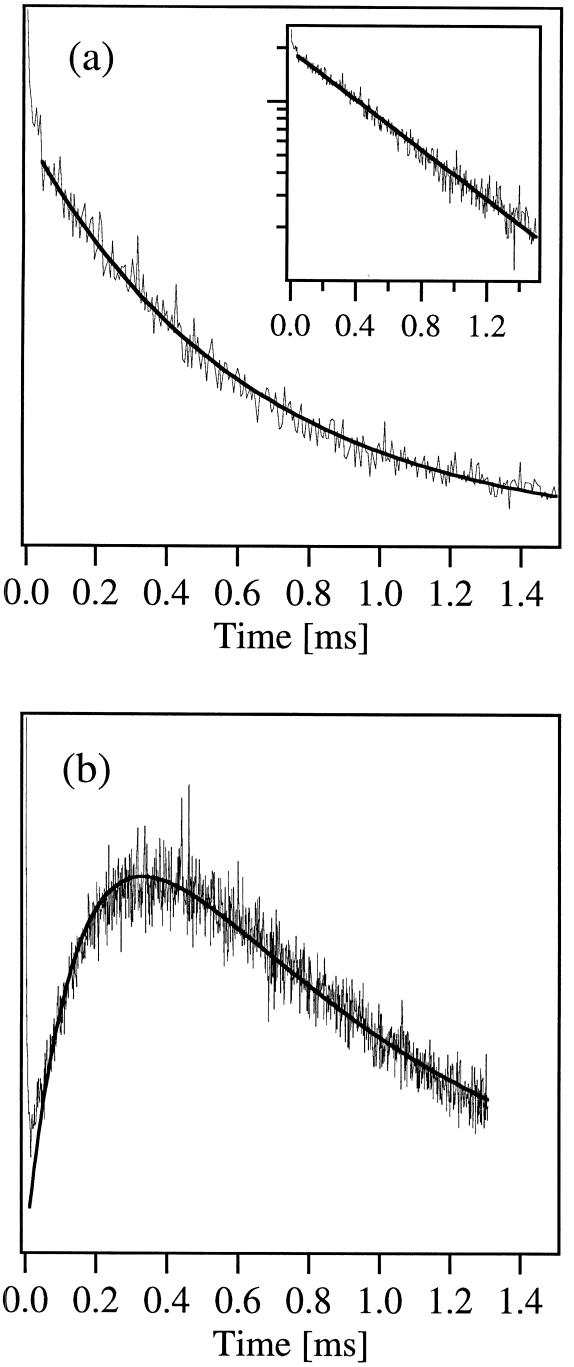

Fig. 14. Time evolution of upconversion luminescence in $CsCdBr_3$:2.25% Ho^{3+} at 100 K after (a) excitation at 11 028 cm^{-1} in the shaded area of Fig. 13 and (b) at 11 232 cm^{-1} in the unshaded area of Fig. 13. The inset in (a) is a semi-logarithmic plot. (Figure reproduced from Ref. [24].)

fluoride lattices. Besides its fundamental importance this research has a materials oriented component. Both for new laser and phosphor materials a NIR to VIS upconversion excitation scheme is an attractive alternative to conventional techniques. Very efficient semiconductor diode lasers are available as potential pump sources. Most of the chloride, bromide and iodide host materials are hygroscopic, which is a significant disadvantage, particularly for laser applications. For phosphor applications encapsulation or an inert working atmosphere should be achievable.

Acknowledgements

We want to thank Markus Hehlen, Karl Krämer, Stefan Lüthi, Philipp Müller, Toni Riedener and Markus Wermuth, who have contributed to this work over the past 10 years. Financial support from the Swiss National Science Foundation is gratefully acknowledged.

References

[1] F.E. Auzel, Proc. IEEE 61 (1973) 758.
[2] J.C. Wright, Top. Appl. Phys. 15 (1976) 239.
[3] T. Sandrock, H. Scheife, E. Heumann, G. Huber, Opt. Lett. 22 (1997) 808.
[4] R. Paschotta, P.R. Barber, A.C. Tropper, D.C. Hanna, J. Opt. Soc. Am. B 14 (1997) 1213.
[5] R.J. Thrash, L.F. Johnson, J. Opt. Soc. Am. B 11 (1994) 881.
[6] R.M. Macfarlane, F. Tong, A.J. Silversmith, W. Lenth, Appl. Phys. Lett. 52 (1988) 1300.
[7] P.E.-A. Möbert, A. Diening, E. Heumann, G. Huber, B.H.T. Chai, Laser Phys. 8 (1998) 214.
[8] L.F. Johnson, H.J. Guggenheim, Appl. Phys. Lett. 20 (1972) 474.
[9] R.A. McFarlane, Appl. Phys. Lett. 54 (1989) 2301.
[10] T.J. Whitley, C.A. Millar, R. Wyatt, M.C. Brierley, D. Szebesta, Electron. Lett. 27 (1991) 1785.
[11] R. Brede, T. Danger, E. Heumann, G. Huber, B.H.T. Chai, Appl. Phys. Lett. 63 (1993) 729.
[12] M.P. Hehlen, K. Krämer, H.U. Güdel, R.A. McFarlane, R.N. Schwartz, Phys. Rev. B 49 (1994) 12475.
[13] A.A. Kaminskii, in: M.J. Weber (Ed.), Crystalline Lasers: Physical Processes and Operating Schemes, CRC Press, Boca Raton, FL, 1996.
[14] S.R. Lüthi, H.U. Güdel, M.P. Hehlen, J.R. Quagliano, Phys. Rev. B 57 (1998) 15229.
[15] M.P. Hehlen, H.U. Güdel, J.R. Quagliano, J. Chem. Phys. 101 (1994) 10303.
[16] S.R. Lüthi, H.U. Güdel, M.P. Hehlen, J. Chem. Phys. 110 (1999) 12033.
[17] J.M.F. van Dijk, M.F.H. Schuurmans, J. Chem. Phys. 78 (1983) 5317.
[18] N.J. Cockroft, G.D. Jones, D.C. Nguyen, Phys. Rev. B 45 (1992) 5187.
[19] S.R. Lüthi, M. Pollnau, H.U. Güdel, M.P. Hehlen, Phys. Rev. B 60 (1999) 162.
[20] M. Pollnau, D.R. Gamelin, S.R. Lüthi, H.U. Güdel, M.P. Hehlen, Phys. Rev. B 61 (2000) 3337.
[21] M.P. Hehlen, H.U. Güdel, Q. Shu, J. Rai, S.C. Rand, J. Chem. Phys. 104 (1996) 1232.
[22] T. Riedener, H.U. Güdel, G.C. Valley, R.A. McFarlane, J. Lumin. 63 (1995) 327.
[23] M. Wermuth, T. Riedener, H.U. Güdel, Phys. Rev. B 57 (1998) 4369.
[24] P. Müller, M. Wermuth, H.U. Güdel, Chem. Phys. Lett. 290 (1998) 105.